

A FINITE ELEMENT MODEL FOR FLUID-STRUCTURE INTERACTION STUDIES

A. N. NAHAVANDI

*Department of Chemical Engineering and Applied Chemistry,
351 Terrace Building, Columbia University, New York, N.Y. 10027, U.S.A.*

SUMMARY

A finite element methodology for fluid-structure interaction studies in wave propagation problems is presented. This methodology is based on the discretization of the Lagrangian equations of motion for the structure and the Eulerian equations of motion for the fluid with structural displacements and fluid pressure and velocity components as the nodal degrees of freedom. The geometric domain of interest, comprising of solid-fluid continua, is first discretized by appropriate subdivisions into an assemblage of interconnected regions defining fluid finite elements, solid finite elements and combined solid-fluid super-elements (covering the solid-fluid boundary regions).

Equations considered for the fluid finite elements are the continuity and the Navier-Stokes equations in Eulerian form for an unsteady compressible two-dimensional flow in conjunction with an equation of state. The present methodology employs the Method of Weighted Residuals by multiplying the discretized fluid equations by a set of weight functions and integrating over the volume of the element. The weight functions are chosen to be identical to the shape functions as indicated by the Galerkin's approach to the finite element formulation.

The solid finite element formulation is developed based on the method of virtual work by equating the work and change in internal energy during a virtual displacement.

The solid-fluid super-element formulation is assembled by combining the solid and fluid elements including the interaction between the two. For the solid element, the interaction term involves mainly the fluid pressure forces acting on the solid boundaries. For the fluid element, the interaction is expressed by making the fluid normal velocity component at the boundary equal to that of the solid.

The elemental matrices for the fluid-element and the solid-fluid super-element are non-symmetric. A direct numerical integration will require excessive computer memory and running time for the storage and algebraic manipulation of the global matrices. For these reasons, the numerical solution is achieved by a combination of matrix decomposition, analytic integration and iterative scheme which allows the application of the elemental matrices, rather than the system global matrices.

The methodology presented herein provides an efficient means for the study of fluid-structure interaction. The application of this methodology to wave propagation problems detect the occurrence of a transverse water hammer which may have important implications in the design of reactor internals.

1. INTRODUCTION

Flow induced vibration of reactor components is of major concern to the utilities, steam supply manufacturers and the regulatory agencies. The concern is based on the impact of long plant outages and the associated loss of the electrical generating capacity, together with the extremely high cost of repairs resulting from fatigue failure or excessive wear of key components caused by flow induced vibration.

It is generally agreed that there are four mechanisms of flow induced vibration. The first called turbulent excitation or buffeting, refers to unsteady forces developed on a body exposed to a highly turbulent flow.

The second mechanism, referred to as acoustic excitation, is associated with the acoustic characteristics of the duct through which the fluid is flowing and involves the sloshing of the fluid across the duct.

The third mechanism called vortex shedding, refers to that even when a bluff body is exposed to a perfectly uniform, nonturbulent incident flow, the wake behind the body develops an instability leading to fluctuating lift and drag forces on the body.

Finally, a flowing fluid can also contribute inertia force, damping force and elastic force to a body vibrating in it. These are effects arising specially from bodies moving in a flow medium and are hence describable as "motion dependent" [1,2,3]. The position of the structure with respect to the incident stream may cause a transverse fluid force on the structure producing instability and self-excited vibration characterized by continual lateral displacements. The forces causing this instability are affected by the deflection of the structure from its undeformed state. This is referred to as fluid elastic excitation, flutter, or galloping. A study of fluid elastic excitations requires the consideration of both solid and fluid motions including their interactive forces and constraints. The purpose of this study is to develop a methodology for the study of the problem of fluid elastic excitation using a finite element approach. This methodology is based on the discretization of the Lagrangian equations of motion for the solid and the Eulerian equations of motion for the fluid with structural displacements and fluid pressure and velocity components as the nodal degrees of freedom.

2. Mathematical Formulation

The geometric domain of interest, comprising of solid-fluid continua, is first discretized by appropriate subdivisions into an assemblage of interconnected regions defining fluid finite elements, solid finite elements and combined solid-fluid super-elements (covering the solid-fluid boundary regions). The mathematical model for each element is then developed as described hereunder:

2.1 Fluid Element

The generalized Navier-Stokes equations for viscous, compressible, isothermal, two-dimensional flow can be written in the following form:

$$\frac{\partial P}{\partial t} + \frac{\partial Q}{\partial x} + \frac{\partial R}{\partial y} = R_e^{-1} \left(\frac{\partial^2 S}{\partial x^2} + \frac{\partial^2 T}{\partial y^2} + \frac{\partial^2 U}{\partial x \partial y} \right) \quad (1)$$

where

$$P = \begin{Bmatrix} \rho \\ \rho v_x \\ \rho v_y \end{Bmatrix}, \quad Q = \begin{Bmatrix} \rho v_x \\ p + \rho v_x^2 \\ \rho v_x v_y \end{Bmatrix}, \quad R = \begin{Bmatrix} \rho v_y \\ \rho v_x v_y \\ p + \rho v_y^2 \end{Bmatrix}$$

$$S = \begin{Bmatrix} 0 \\ 4/3\mu v_x \\ \mu v_y \end{Bmatrix}, \quad T = \begin{Bmatrix} 0 \\ \mu v_x \\ 4/3\mu v_y \end{Bmatrix}, \quad U = \begin{Bmatrix} 0 \\ -1/3\mu v_y \\ -1/3\mu v_x \end{Bmatrix} \quad (2)$$

and

$$p = p(\rho) \quad (3)$$

where v_x , v_y are fluid velocity components in x and y directions and p , ρ , μ , and R_e are the fluid pressure, density, viscosity and Reynolds Number. Employing the Method of Weighted Residuals requires that the weighted integral of the differential equation to be zero over the finite element domain A :

$$\int_A W_i \left[\frac{\partial P}{\partial t} + \frac{\partial Q}{\partial x} + \frac{\partial R}{\partial y} - R_e^{-1} \left(\frac{\partial^2 S}{\partial x^2} + \frac{\partial^2 T}{\partial y^2} + \frac{\partial^2 U}{\partial y \partial x} \right) \right] dA = 0 \quad (4)$$

where W_i is an arbitrary weighting function. Expressing the flow variables in terms of the product of the shape function and the nodal flow variables, one obtains

$$\begin{aligned} P &= N_j^P P_j & Q &= N_j^Q Q_j & R &= N_j^R R_j \\ S &= N_j^S S_j & T &= N_j^T T_j & U &= N_j^U U_j \end{aligned} \quad (5)$$

substituting Eqs. (5) into Eq. (4) and integrating the last five terms of this equation by parts, yields

$$\begin{aligned} &\int_A \left[W_i N_j^P \dot{P}_j - \frac{\partial W_i}{\partial x} N_j^Q Q_j - \frac{\partial W_i}{\partial y} N_j^R R_j \right. \\ &\quad \left. + R_e^{-1} \left(\frac{\partial W_i}{\partial x} \frac{\partial N_j^S}{\partial x} S_j + \frac{\partial W_i}{\partial y} \frac{\partial N_j^T}{\partial y} T_j + \frac{\partial W_i}{\partial x} \frac{\partial N_j^U}{\partial y} U_j \right) \right] dx dy \\ &+ \int_C W_i \left[Q l_x + R l_y - R_e^{-1} \left(l_x \frac{\partial S}{\partial x} + l_y \frac{\partial T}{\partial y} + l_x \frac{\partial U}{\partial y} \right) \right] ds \end{aligned} \quad (6)$$

where l_x , l_y are the cosine directors of the outward unit normal to the boundary segment ds . It should be noted that many authors choose to integrate by parts only the terms involving the second-order spatial-derivatives [4] while others prefer to integrate by parts both the first- and the second-order spatial derivatives. The former approach results in an unsymmetric influence matrix while the latter leads to a symmetric matrix.

Defining the following element matrices and array:

$$\begin{aligned} [A_{ij}^e] &= \int_A W_i N_j^P dA & [B_{ij}^e] &= - \int_A \frac{\partial W_i}{\partial x} N_j^Q dA \\ [C_{ij}^e] &= - \int_A \frac{\partial W_i}{\partial y} N_j^R dA & [D_{ij}^e] &= R_e^{-1} \int_A \frac{\partial W_i}{\partial x} \frac{\partial N_j^S}{\partial x} dA \\ [E_{ij}^e] &= R_e^{-1} \int_A \frac{\partial W_i}{\partial y} \frac{\partial N_j^T}{\partial y} dA & [F_{ij}^e] &= R_e^{-1} \int_A \frac{\partial W_i}{\partial x} \frac{\partial N_j^U}{\partial y} dA \end{aligned} \quad (7)$$

and

$$\{G_i\} = - \int_C W_i \left[Q l_x + R l_y - R_e^{-1} \left(l_x \frac{\partial S}{\partial x} + l_y \frac{\partial T}{\partial y} + l_x \frac{\partial U}{\partial y} \right) \right] ds \quad (8)$$

Eq. (6) reduces to

$$\begin{aligned} [A_{ij}^e] \{ \dot{P}_j \} + [B_{ij}^e] \{ Q_j \} + [C_{ij}^e] \{ R_j \} &+ \\ [D_{ij}^e] \{ S_j \} + [E_{ij}^e] \{ T_j \} + [F_{ij}^e] \{ U_j \} &= \{ G_i \} \end{aligned} \quad (9)$$

Eq. (9) is a set of ordinary differential equations for an element e . It is often more convenient to compute the element matrices (Eqs. 7) in terms of the local element coordinate system (ξ, η) . This purpose can be achieved by using the following coordinate transformation:

$$dA = dx dy = \Delta_J d\xi d\eta \quad (10)$$

$$\begin{Bmatrix} \frac{\partial f}{\partial x} \\ \frac{\partial f}{\partial y} \end{Bmatrix} = [\mathbf{J}]^{-1} \begin{Bmatrix} \frac{\partial f}{\partial \xi} \\ \frac{\partial f}{\partial \eta} \end{Bmatrix} \quad (11)$$

where

$$[\mathbf{J}] = \begin{bmatrix} \frac{\partial x}{\partial \xi} & \frac{\partial y}{\partial \xi} \\ \frac{\partial x}{\partial \eta} & \frac{\partial y}{\partial \eta} \end{bmatrix} \quad (12)$$

in which Δ_J is the determinant of the Jacobian matrix \mathbf{J} . The resulting integral evaluation may be performed numerically using high order Gaussian quadrature formulas.

To verify the above derivation, the fluid element matrix equation was derived for a subset of Navier-Stokes and continuity equations valid for a weak wave approximation given by Continuity equation:

$$\frac{\partial \rho}{\partial t} + \rho_f \left(\frac{\partial v_x}{\partial x} + \frac{\partial v_y}{\partial y} \right) = 0 \quad (13)$$

Momentum equation:

$$\frac{\partial v_x}{\partial t} = -\frac{1}{\rho_f} \frac{\partial P}{\partial x} - k_f v_x \quad (14)$$

$$\frac{\partial v_y}{\partial t} = -\frac{1}{\rho_f} \frac{\partial P}{\partial y} - k_f v_y \quad (15)$$

Equation of state:

$$\left(\frac{\partial P}{\partial \rho_s} \right) = c^2 = \text{constant} \quad (16)$$

In this approximation, the momentum flux terms in the equations of motions are neglected and the fluid viscous effects are considered to be proportional to their respective velocity components. These assumptions permit the verification of the results with previous solid-fluid interaction studies based on a two-dimensional wave equation [5]. Eliminating ρ between Eqs. (13) and (16) and performing the operations indicated earlier, Eq. (9) reduces to

$$[\mathbf{H}_{ij}^e] \{ \dot{Z} \} + [\mathbf{L}_{ij}^e] \{ Z \} = 0 \quad (17)$$

in which $[\mathbf{H}_{ij}^e]$ and $[\mathbf{L}_{ij}^e]$ are the unsymmetric fluid inertia and fluidity matrices for the fluid element, $\{Z\}$ is the elemental array involving nodal degrees of freedom (pressure, x-component of velocity, and y-component of velocity, and $\{\dot{Z}\}$ is the time derivative of $\{Z\}$.

2.2 Solid Element

The solid finite element is obtained by applying the principle of virtual work to the solid [6, 7]. This procedure yields the well-known matrix differential equation for the nodal displacements of the solid element given by

$$[\mathbf{M}_{ij}^e] \{ \ddot{X} \} + [\mathbf{C}_{ij}^e] \{ \dot{X} \} + [\mathbf{K}_{ij}^e] \{ X \} = \{ R \} \quad (18)$$

where $[\mathbf{M}_{ij}^e]$, $[\mathbf{C}_{ij}^e]$ and $[\mathbf{K}_{ij}^e]$ are the solid element mass, damping and stiffness matrices and $\{\ddot{X}\}$, $\{\dot{X}\}$, $\{X\}$ and $\{R\}$ are the solid element acceleration, velocity, displacement and

external force arrays.

2.3 Solid-Fluid Super-Element

The solid-fluid super-element, typically shown in Figs. 1 and 2, is constructed by combining the solid and fluid elements while at the same time including the interaction between the two elements. For the solid element, the main interaction term is the pressure force acting normal to the moving solid boundary. The contribution of viscous effects in the boundary conditions is sufficiently small to be neglected. For the fluid element, the interaction is expressed by making the fluid velocity component normal the boundary equal to the corresponding solid velocity component. The matrix differential equation for the solid-fluid super-element becomes

$$\begin{bmatrix} M_{ij}^e & 0 \\ 0 & 0 \end{bmatrix} \begin{Bmatrix} \ddot{X} \\ \ddot{Z} \end{Bmatrix} + \begin{bmatrix} c_{ij}^e & 0 \\ 0 & H_{ij}^e \end{bmatrix} \begin{Bmatrix} \dot{X} \\ \dot{Z} \end{Bmatrix} + \begin{bmatrix} K_{ij}^e & 0 \\ 0 & L_{ij}^e \end{bmatrix} \begin{Bmatrix} X \\ Z \end{Bmatrix} = \begin{Bmatrix} [S_e] \\ 0 \end{Bmatrix} p \quad (19)$$

where the solid-fluid coupling matrix $[S_e]$ is given in terms of the solid boundary shape function $[\bar{N}_s]$ and fluid shape functions $[N_f]$ by [5] :

$$[S_e] = \int_s [\bar{N}_s]^T [N_f] ds \quad (20)$$

together with constraint that for nodal points on the solid-fluid boundary

$$\begin{Bmatrix} v_y \end{Bmatrix} = \begin{Bmatrix} \dot{u}_y \end{Bmatrix} \quad (21)$$

The elemental matrices for the fluid element and the solid-fluid super-element are non-symmetric. This precludes the application of the highly efficient modal superposition technique with real eigenvalues and orthogonal eigenvectors. A direct numerical integration would require excessive computer memory and running time for the storage and algebraic manipulation of the global matrices. For these reasons, the numerical solution is obtained by a combination of matrix decomposition, analytic integration and iterative scheme [8] which allows the application of the elemental matrices, rather than the system global matrices.

2. PRESENTATION OF RESULTS

The finite element model developed in this study (designated as multi-variable pressure-velocity formulation) is verified for a two-dimensional channel flow with elastic walls shown in Fig. 2. The results obtained are compared with a previous study based on a finite element model with pressure considered as the only dependent variable in the fluid region (referred to as the single-variable pressure formulation [5]). The results are also compared with channel flow between two rigid parallel plates. Water initially at rest is accelerated suddenly by applying a step pressure, p_0 at the left end while maintaining a zero pressure at the right end. A 72 element grid model is used in this analysis. Elements 6, 15, 24, 33, 42, 51, 60 and 69 are modeled using the solid-fluid quadrilateral super-elements. Elements located below and above these elements are modeled employing fluid and solid triangular finite elements respectively. Two values of fluid viscous damping are studied: 1) Inviscid case, $k_f = 0.$, and 2) Highly viscous case, $k_f = 3062.467 \text{ sec}^{-1}$.

A special-purpose digital computer program is employed to solve the problem. Response time histories are obtained numerically for the cases indicated above. Typical nodal pressure and velocity components for the fluid and the nodal displacement components for the solid for one position upstream are plotted for the present study employing the multi-

variable pressure-formulation and compared with two previous studies: 1) single-variable pressure-formulation based on two-dimensional wave propagation between elastic walls (see Figs. 3 and 4); and 2) multi-variable pressure-velocity formulation for two-dimensional wave propagation between rigid walls and simplified one-dimensional analytical solution for channel flow with rigid walls (see Figs. 5 and 6). The positions and variables selected for plotting are marked on each figure and the physical data are summarized in Table 1.

To establish the convergence of the numerical solution, the minimum period associated with the smallest length increment is calculated from

$$T_{\min} = 2 \pi \frac{l_{\min}}{c} \quad (22)$$

Since the speed of sound in the solid is much larger than that of the fluid and the solid length increments are much smaller than that of the fluid, the minimum period will correspond to the solid element with the smallest length. For $l_{\min} = 0.25$ inches and $c = 2.0276 \times 10^5$ in/sec, T_{\min} becomes equal to 7.75×10^{-6} sec. To ascertain the convergence of the solution, the integration time step was kept much smaller than this minimum period. The convergence of the solution was established when doubling the time interval produced no significant change in the model time histories.

Figures 3 and 4 show a comparison of the multi-variable pressure-velocity formulation, employed in this study, with single-variable pressure-formulation from reference [5] based on the two-dimensional wave equation. The two solutions are generally in reasonable agreement. However, since the velocity components are not among the system degrees of freedom in the single-variable pressure formulation, the associated time responses cannot be expected to be as accurate as the present multi-variable pressure-velocity formulation.

It should be remembered that the velocity time responses, shown in Fig. 4, are the distinctive features of the multi-variable pressure-velocity formulation presented herein since the single-variable pressure formulation can provide only an elemental velocity calculated from the nodal pressures. A comparison between the multi-variable and single-variable velocity time histories has been made possible by averaging the nodal velocities from the multi-variable study and comparing the result with the elemental velocity from the single-variable approach which show a good agreement. This verification provides the confidence needed to initiate further parametric studies.

The typical solid vertical displacement, fluid pressure, and axial and transversal fluid velocity time histories at the wall are presented at one upstream location for inviscid case in Figs. 5 and 6. Superimposed on these curves are two rigid wall (no solid-fluid interaction) curves for comparison. The first is a finite element solution for the wave propagation problem with rigid walls using multi-variable pressure-velocity formulation. The second is the analytic solution to the one-dimensional wave equation for the rigid wall problem [9].

In Fig. 5, the pressure time history for the multi-variable pressure-velocity formulation in the rigid wall case oscillate about the simplified one-dimensional analytically-calculated rectangular wave form. However, the simplified one-dimensional analytical solution allows only axial motion or pressure variation and, therefore, cannot be expected to be accurate for a two dimensional flow field under consideration. The multi-variable pressure velocity formulation with rigid walls allows a two-dimensional pressure and velocity variation and

for this reason, the pressure response is more oscillatory. This oscillatory behavior has been observed by other investigators both experimentally and analytically [10, 11, 12, 13]. For the elastic wall case, the pressure surge in the channel results in a gradual deflection of the wall leading to a reduction of the axial pressure surge which is initially more pronounced near the wall than at the center. This situation creates a transverse flow, as shown in Fig. 6, until the wall deflection reaches a maximum and no longer permits a transverse flow leading to a transversal water hammer and pressure surge about $t^L/c = 2$ which is distinctly opposed to the zero pressure dip for the rigid wall case. The transversal pressure surge occurs first at the wall and then travels backward to the centerline. This transversal water hammer has a substantial effect on the response characteristics and may have important implications in the design of fluid systems. Following the transverse surge phenomenon, the elastic energy stored in the wall forces the wall to move back toward its initial position and reverses the transverse flow direction with a subsequent gradual pressure rise toward the end of the cycle. The axial flow, for the elastic wall case, is larger than that of the rigid wall as the wall deflects outward and is smaller as the wall moves inward. This behavior is more pronounced near the wall (element 24 in Fig. 6) than near the channel centerline.

In comparison with the inviscid flow case, the pressure, velocity and displacement amplitudes in the highly viscous flow case (not shown) are lower and the curves are smoother as expected. The transverse surge is not as large and the solution tends toward a steady-state value corresponding to the rigid wall case because of the highly viscous flow conditions.

Table 1. Physical Data for the Elastic Wall Case

Parameters	British Unit	SI Unit
Fluid density	9.35521×10^{-5} lbf-sec ² /in ⁴	999.78 N-sec ² /m ⁴
Solid density	7.297×10^{-4} lbf-sec ² /in ⁴	7798.2 N-sec ² /m ⁴
Speed of sound in fluid	6.0×10^4 in/sec	1524.0 m/sec
Speed of sound in solid	2.0276×10^5 in/sec	5150.1 m/sec
Solid Young Modulus	30.0×10^6 psi	20.68×10^7 kPa
Solid Poisson Ratio	0.3	0.3
Pressure at channel inlet	10 psia	68948.0 Pa
Channel length, L	29.4 in	0.747 m
Channel height, h	24.0 in	0.610 m
Wall thickness, w	0.5 in	0.0127 m

4. REFERENCES

- /1/ Savkar, S.D., "A Survey of Flow Induced Vibrations of Cylindrical Arrays in Cross Flow". ASME publication 76-WA/FE-21 for meeting of Dec. 5, 1976.
- /2/ Chen, S.S., "Flow-Induced Vibration of Circular Cylindrical Structures, Part I: Stationary Fluids, and Parallel Flow", The Shock and Vibration Digest, Vol. 9, No. 10, October 1977, pp. 25-38.
- /3/ Chen, S.S., "Flow-Induced Vibration of Circular Cylindrical Structures, Part II: Cross-Flow Considerations", The Shock and Vibration Digest, Vol. 9, No. 11, November 1977, pp. 21-28.

- /4/ Huebner, K.H., The Finite Element Method for Engineers, John Wiley and Sons, New York, 1975, p. 343.
- /5/ Nahavandi, A.N. and Pedrido, R.R., "An Analysis of Solid-Fluid Interaction Using the Finite Element Method". Dynamic Analysis of Pressure Vessel and Piping Components, ASME PVP-PB-022, 1977, pp. 75-93.
- /6/ Zienkiewicz, O.C., The Finite Element Method in Engineering Science, McGraw-Hill, London, 1971.
- /7/ Przemieniecki, J.S., Theory of Matrix Structural Analysis, McGraw-Hill, New York, 1968.
- /8/ Nahavandi, A.N. and Falsafi, R. "Interaction Between Structures and Fluids". Proceedings of the ASME Symposium on Flow-Induced Vibration, San Francisco, Cal., June 25-29, 1979.
- /9/ Nahavandi, A.N., Bohm, G.J. and Pedrido, R.R., "Structurally Compatible Fluid Finite Element for Solid-Fluid Interaction Studies", Nuclear Engineering and Design, Vol. 35, 1975, pp. 335-347.
- /10/ Conway, H.D. and Jakubowski, M., "Axial Impact of Short Cylindrical Bars", ASME publication 69-WA/APM-6 for meeting of November 16-20, 1969.
- /11/ Zielke, W., "Frequency-Dependent Friction in Transient Pipe Flow", Transactions of ASME, Journal of Basic Engineering, March 1968, pp. 109-115.
- /12/ Holmboe, E.L. and Rouleau, W.T., "The Effect of Viscous Shear on Transients in Liquid Lines", Transactions of ASME, Journal of Basic Engineering, Vol. 89, No. 1, March 1967, 174-180.
- /13/ Tarantine, F.J. and Rouleau, W.T., "Fluid Pressure Transients in a Tapered Transmission Line", Transactions of ASME, Journal of Basic Engineering, Vol. 89, No. 1, March, pp. 181-190.

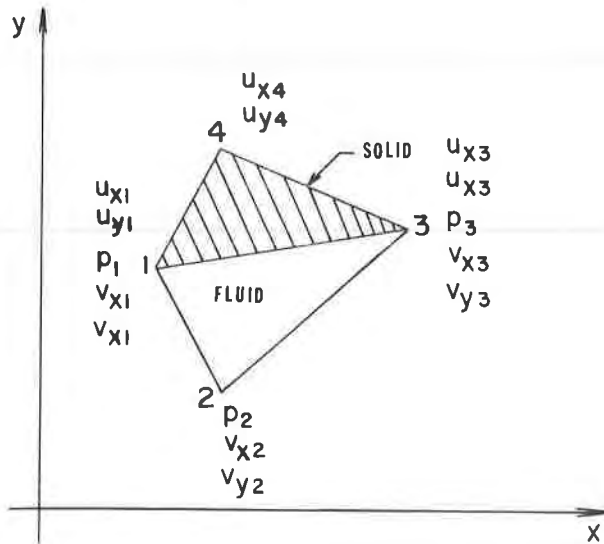


Fig. 1 Plane Quadrilateral Solid-Fluid Super-element

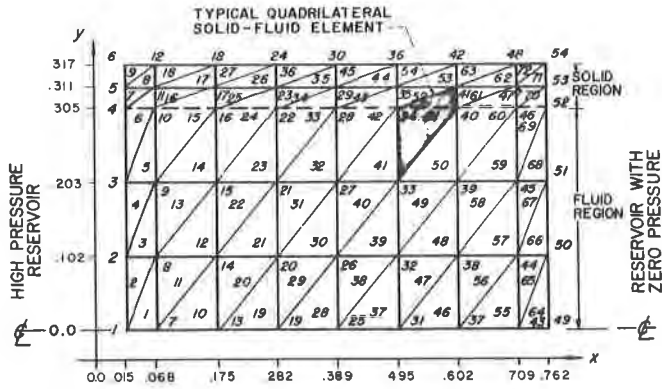


Fig. 2 72 Element Solid-Fluid Model

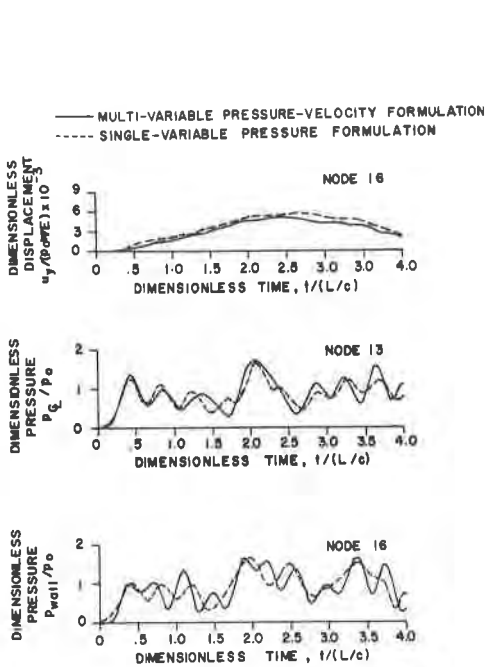


Fig. 4 A Comparison of Multi- and Single-Variable Fluid Velocity Time Histories for Elastic Wall Case with Inviscid Flow (at $x = 0.175m$)

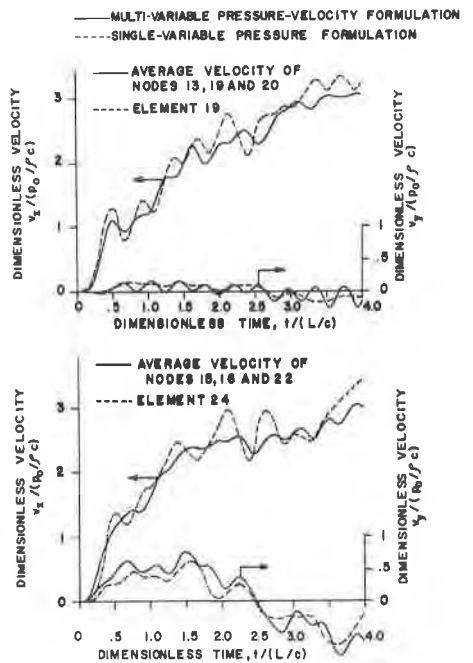


Fig. 3 A Comparison of Multi- and Single-Variable Pressure and Displacement Time Histories for Elastic Wall Case with Inviscid Flow (at $x = 0.175m$)

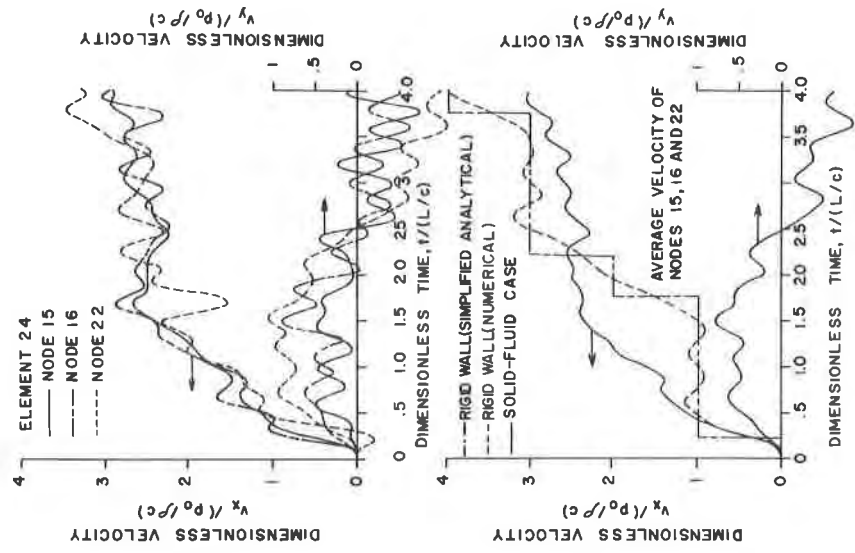


Fig. 6 A Comparison of Fluid Velocity Time Histories for Elastic and Rigid Wall Cases with Inviscid Flow (at $x = 0.175$ m near the wall)

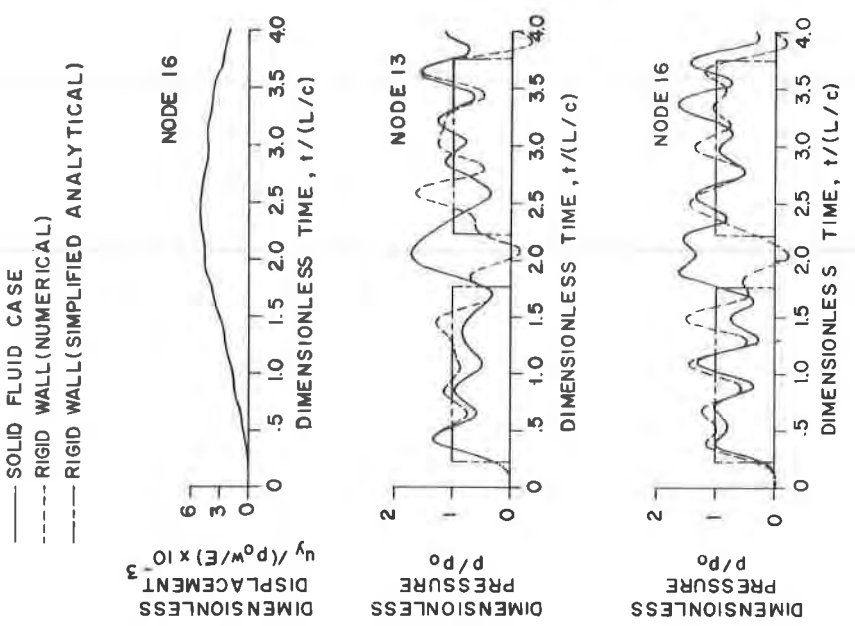


Fig. 5 A Comparison of Pressure and Displacement Time Histories for Elastic and Rigid Wall Cases with Inviscid Flow (at $x = 0.175$ m)